RSC Advances

RSC Publishing

PAPER

View Article Online
View Journal | View Issue

Cite this: *RSC Advances*, 2013, **3**, 3611

Nano-MgO–ZrO_2 mixed metal oxides: characterization by SIMS and application in the reduction of carbonyl compounds and in multicomponent reactions†

Manoj B. Gawande,*[a] Anuj K. Rathi,[b] Paula S. Branco,[a] T. M. Potewar,[a] Alexandre Velhinho,[c] Isabel D. Nogueira,[d] Alexander Tolstogouzov,[e] C. Amjad A. Ghumman[e] and Orlando M. N. D. Teodoro[e]

Received 13th October 2012,
Accepted 4th January 2013

DOI: 10.1039/c2ra22511e

www.rsc.org/advances

A nano-sized Magnesia–Zirconia (nano-MgO–ZrO_2) catalyst was prepared by a simple ultradilution co-precipitation method and by using inexpensive precursors. The nano-MgO–ZrO_2 was extensively characterized by SIMS together with other analytical techniques such as X-ray diffraction (XRD) and transmission electron microscopy (TEM). The nano-MgO–ZrO_2 catalyst proved to be very efficient for the reduction of carbonyl compounds and multicomponent reactions under mild reaction conditions. The recyclability and reusability of the nano-MgO–ZrO_2 catalyst has been tested.

Introduction

Mixed metal oxides (MMOs) represent one of the most important and widely employed categories of solid catalysts, either as active phases or supports. MMOs may be used either by their acid/base or their redox properties and constitute the largest family of heterogeneous catalysts.[1–3] In addition to catalytic applications, MMOs have played very important roles in many areas such as in chemistry, physics, materials science, and geochemistry.[4–6] Due to their versatile applications, they have great scope in various microelectronic devices, electrodes and sensors.[7] Nano-sized MMOs are attractive for a range of applications due to their excellent chemical and thermal stability, high porosity and large surface area. Therefore, great efforts are dedicated to the optimization of new procedures able to synthesize pure and mixed nano-sized metal oxides. MMOs have been used for the selective reduction of the C=O bond in α,β-unsaturated carbonyl compounds through hydrogen transfer reactions,[8a] the study of chemical structures and performance of perovskite oxides,[8b] the epoxidation of allyl acetate with *tert*-butyl hydroperoxide catalyzed by MoO_3/TiO_2 oxide,[8c] and the determination of the effect of the phosphate ion on the textural and catalytic activity of titania–silica mixed oxide,[8d] among other relevant applications in chemistry.[8e–i]

The reduction of carbonyl compounds to their corresponding alcohols is an industrially important reaction, as alcohols are important starting materials and intermediates for the manufacture of a variety of chemicals.[9] Although a number of methods have been developed for the reduction of carbonyl compounds employing homogeneous catalysts,[10] the control of the reaction rates is highly difficult.[11] Moreover, the main disadvantage of these reactions is that when homogeneous catalysts are used, the metal can contaminate the product, which is unacceptable *e.g.* in pharmaceutical syntheses. Recently, prompted by stringent environment protection laws, there has been an increased emphasis on the design, synthesis and use of environmentally benign solid acid/base heterogeneous catalysts for organic transformations to reduce the amount of toxic waste and by products from chemical processes. The main advantage of a heterogeneous catalyst is that, being a solid material, it is easy to separate from the gas or liquid phase reactants and products after completion of the reaction.

We have previously shown that a MgO–ZrO_2 catalyst has applicability in various important organic reactions such as cross-aldol condensation, *N*-benzyloxycarbonylation of amines, reduction of aromatic nitrocompounds, and synthesis of 1,5-benzodiazepines[12] and *N*-benzyloxycarbonylation of alcohols.[13] Engaged with the development of sustainable protocols,[14] heterogeneous catalysis[15] and nanomaterials,[16] we herein report an extension of the application of the nano-MgO–ZrO_2 catalyst for the reduction of carbonyl compounds

[a]*Department of Chemistry, Faculty of Science and Technology, Universidade Nova de Lisboa, 2829-516 Caparica, Portugal. E-mail: mbgawande@yahoo.co.in, m.gawande@fct.unl.pt; Fax: +351 21 2948550; Tel: +351 96 4223243 Tel: +351 21 2948300*
[b]*Jubilant Chemsys Ltd., B-34, Sector-58, Noida-201301, New Delhi (India)*
[c]*CENIMAT/I3N Departmento de Ciências dos Materiais, Faculdade de Ciências e Tecnologia, FCT, Universidade Nova de Lisboa, 2829-516 Caparica, Portugal*
[d]*Instituto de Ciencia e Engenharia de Materiais e Superficies IST, Lisbon, Portugal*
[e]*Centre for Physics and Technological Research (CeFITec), Department of Physics, Faculty of Science and Technology, Universidade Nova de Lisboa, 2829-516 Caparica, Portugal*

† Electronic supplementary information (ESI) available. See DOI: 10.1039/c2ra22511e

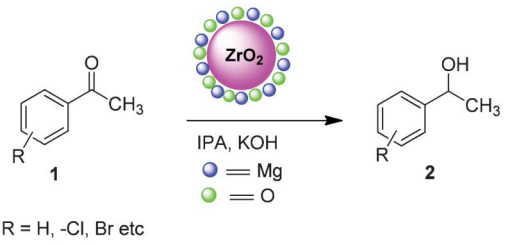

Scheme 1 Reduction of carbonyl compounds by hydrogen transfer reactions over nano-MgO–ZrO_2 catalyst.

using isopropyl alcohol (IPA) as a hydrogen transfer reagent (Scheme 1). In addition to the usually used techniques for the characterization of solid matrixes such as XRD or TEM, we engaged in a extensive chemical characterization of the nano-MgO–ZrO_2 catalyst surface by time of flight secondary mass spectrometry (TOF-SIMS). The TOF-SIMS technique is widely and successfully used to determine the elemental and molecular composition of the surface and near-surface layers of different catalysts.[17]

To produce a plain and conductive sample suitable for SIMS analysis, the powder catalyst was pressed onto an ultra-pure indium foil by Goodfellow (Huntingdon, UK). We used a manual toggle pressing machine by Brauer (Milton Keynes, UK). The sample was prepared by a reported procedure[18] and the TOF-SIMS analysis was performed by acquiring positive and negative secondary ion spectra in the mass range of 0.5–200 *m*/*z*.

Results and discussion

The XRD spectrum of MgO–ZrO_2 is depicted in Fig. 1. Cubic ZrO_2 and MgO phases (according to JCPDS files 49–1642 and 45–0946, respectively) were observed in powder diffraction patterns of MZ, showing the presence of both substances in the sample.

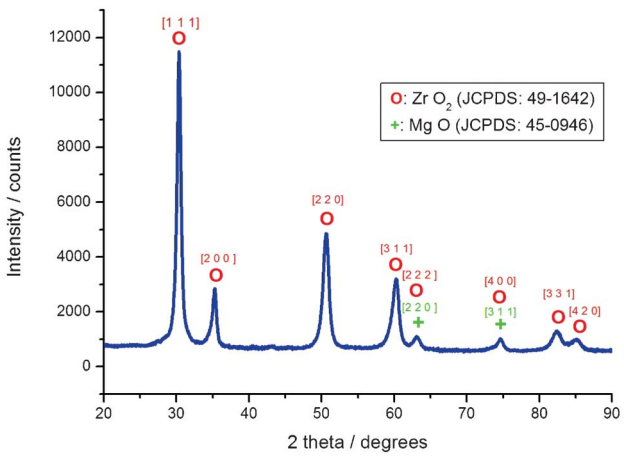

Fig. 1 XRD spectrum of nano-MgO–ZrO_2.

The TEM micrographs of MgO–ZrO_2 are depicted below, clearly indicating that the particles are in the nano-size range (20–35 nm) (Fig. 2a and b). The scarcity of observed particles notwithstanding, it was possible to measure a sufficiently high number to build the histogram (Fig. 2c). In EDS spectra the elements Zr, Mg and O were identified, the results being in general agreement with the XRD spectrum, even if it should be noted that the EDS signal in the TEM analysis concerns a much smaller area. One of the EDS spectra acquired is depicted in Fig. 2d. The copper peak is due to the instrument's grid.

Fig. 3 shows the results obtained from mass spectroscopy, as applied to the MgO/ZrO_2 powder catalyst when placed onto a indium substrate.

In the positive mode (Fig. 3a), we detected the isotopic peaks of the main components and their oxy-hydrated compounds, namely, Mg^+, MgO^+, $MgOH^+$, Zr^+, ZrH^+, ZrO^+, $ZrOH^+$, ZrO_2^+ and ZrO_2H^+, along with some surface contaminations (Na^+, Al^+, K^+, Ca^+), implanted and re-sputtered analysis ions (Ga^+) and ions originating from the substrate (In^+). The intensity of $MgOH^+$ (*m*/*z* 41) is higher than that of MgO^+ (*m*/*z* 40). In the negative mode (Fig. 3b), the isotopic peaks of zirconium oxides and hydroxides with the most abundant peaks at *m*/*z* 122 ($^{90}ZrO_2^-$) and *m*/*z* 123 ($^{90}ZrO_2H^-$ + $^{91}ZrO_2^-$) were registered. At the low-mass part of the spectrum, we detected different hydrocarbons and halogens (F^-, Cl^-); oxygen-containing ions of the analysis (GaO^- and GaO_2^-) and substrate (InO^- and InO_2^-) species were also found. In addition to the abovementioned ions, trace amounts of glycerol were also identified *via* the discrete series of foremost characteristic peaks at *m*/*z* 93 $[M + H]^-$, *m*/*z* 185 $[2M + H]^-$ (not shown), and *m*/*z* 277 $[3M + H]^-$.[18c] We suspect the presence of some glycerol contamination in our vacuum chamber due to the memory effect.

The modification (degradation) of the surface of the catalyst under ion-beam sputtering was studied by measuring four successive positive mass spectra. Each spectrum was collected after short-run Ga^+ pre-sputtering of the sample in the continuous mode. The relative magnesium (zirconium) intensity $RI_{Mg(Zr)}$ was estimated as

$$RI_{Mg(Zr)} = \frac{I_{Mg(Zr)}}{I_{Mg} + I_{Zr}} \quad (1)$$

where $I_{Mg(Zr)}$ is the peak intensity (sum of all isotopes) of the corresponding element integrated within ± 0.5 *m*/*z*.

In Fig. 4 the magnesium and zirconium intensities *versus* the relative gallium calculated intensity is presented

$$RI_{Ga} = \frac{I_{Ga}}{I_{Ga} + I_{Mg} + I_{Zr}} \quad (2)$$

where I_{Ga} is the peak intensity (sum of all isotopes) of Ga^+ analysis ions integrated within ± 0.5 *m*/*z*.

One can see in Fig. 4 that the Mg^+ relative intensity tends to decrease (with corresponding growth of Zr^+ intensity) under

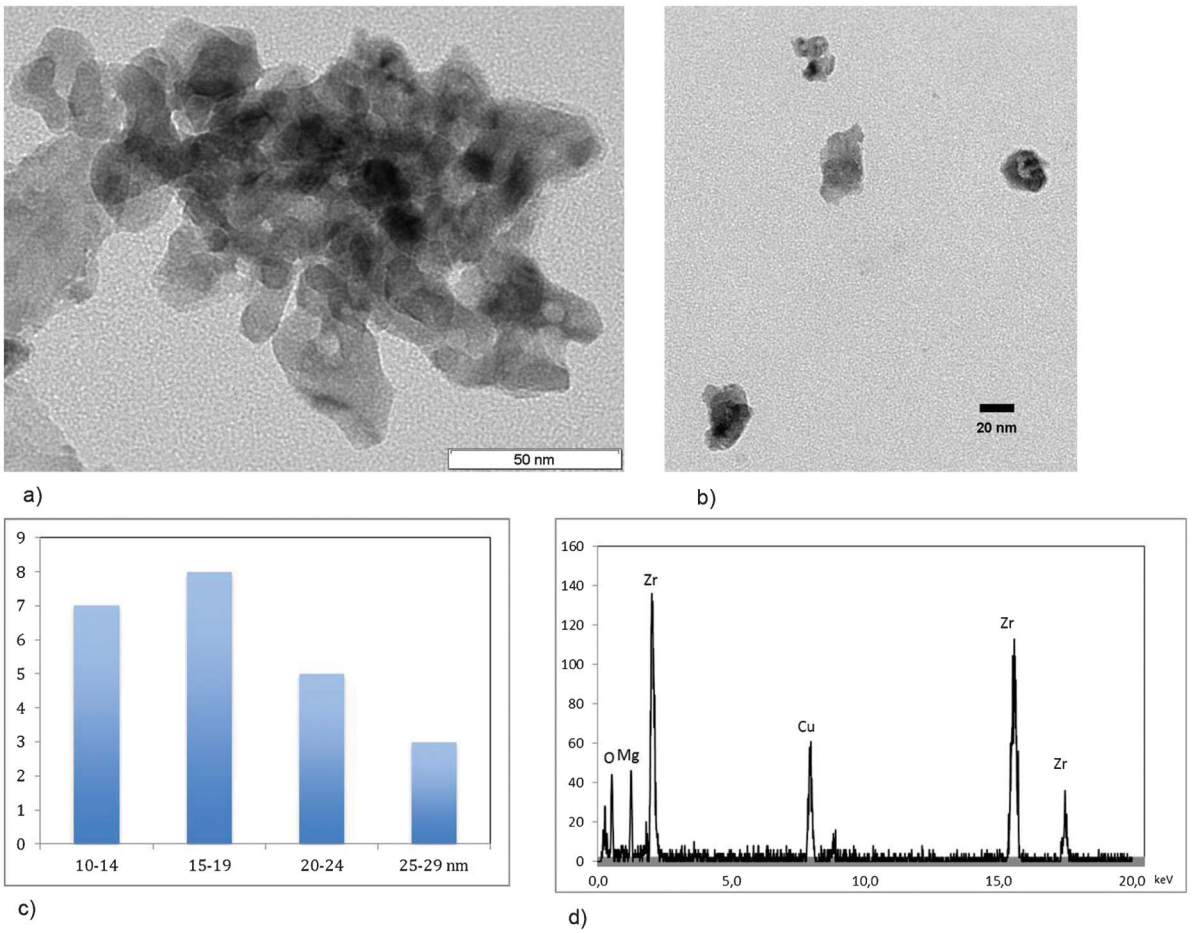

Fig. 2 a) TEM image of nano-MgO–ZrO_2 at 50 nm, b) TEM image of nano-MgO–ZrO_2 at 20 nm, c) histogram of nano-MgO–ZrO_2, d) TEM-EDS profile of nano-MgO–ZrO_2.

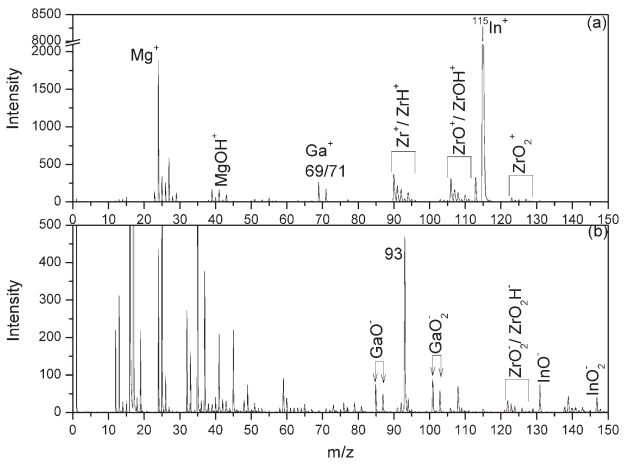

Fig. 3 Mass spectra of positive (a) and negative (b) secondary ions of MgO/ZrO_2 powder catalyst placed onto In substrate. The time of the spectra acquisition was 5 min.

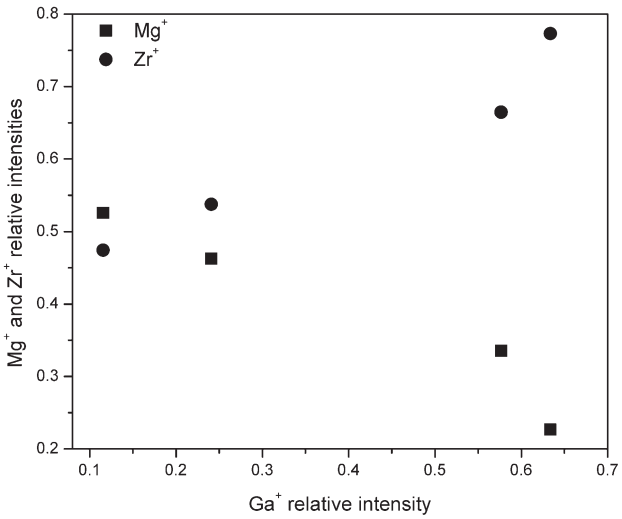

Fig. 4 Relative magnesium and zirconium intensities *versus* the relative Ga^+ content onto the surface of catalysts.

the continuous Ga^+ irradiation, *i.e.* as data is gathered from regions increasingly deeper in the sample. It means that the near-surface region of the catalyst is enriched by Mg. We did not find data on sputter rates of magnesia and zirconia in the literature. However, the sputter rates of aluminum and hafnium oxide films are rather similar,[19] and with a high degree of certainty we are able to ignore the effect of preferential ion-beam sputtering of our samples.

The fact that Mg is preferably found near the surface of the nano-particles is a strong indication that these possess a zirconia-rich core, whereas MgO is mainly present as an adhered deposit at the surface. Whether such deposit assumes the form of a continuous layer, or if magnesia is present over a discrete number of *loci*, could not be ascertained by the experimental techniques used in this study. However, the literature provides examples of systems prepared *via* techniques similar to the ultra-dilution co-precipitation technique possessing a discontinuous deposit structure.[20]

Catalytic activity of MgO–ZrO_2 for carbonyl compound reduction

The catalytic activity of the nano-MgO–ZrO_2 catalyst was tested in the reduction of carbonyl compounds (Scheme 2). For optimization of reactions conditions, we chose acetophenone (**1**, R = H) as the substrate for the reduction under different reaction conditions.

No reactions occur in the absence of catalyst, either with or without base (Table 1, entry 1 and 2). As we increased the amount of catalyst from 10, 20 and 30 mg, we observed the yield of reaction increasing to 42, 68 and 92% respectively (Table 1, entries 4 to 6). The wt% of nano-MgO–ZrO_2 catalyst also affects the reaction rate. It was observed that component oxides such as MgO and ZrO_2 also gave moderate yield of the corresponding products; nevertheless, nano-MgO–ZrO_2 is the most effective nanomaterial among them. This could be due to a prominent feature of the active Mg–Zr mixed oxides, which can be found to originate from the co-operative action of both the basic (O^{2-}) and acidic sites (Mg^{2+} and Zr^{4+}) located in a neighbour at the surface.[21] Even current (micro-size) MgO–ZrO_2 has less catalytic activity in terms of yield of the product (Table 1, entry 9).

The catalytic activity of the nano-MgO–ZrO_2 was further explored for various other carbonyl compounds (Table 2).

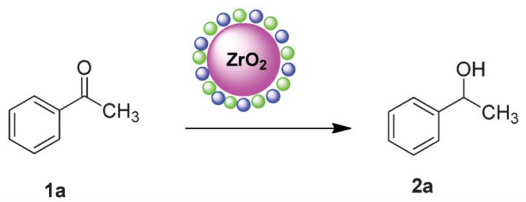

Scheme 2 Aromatic carbonyl group reduction over nano-MgO–ZrO_2.

Table 1 Optimization of reactions conditions[a]

No	Catalyst	Base	Time (h)	Isolated Yield **2a**[d] (%)
1	—	—	24	NR
2	—	KOH	24	NR
3	Nano-MgO-ZrO_2	—	24	NR
4	Nano-MgO-ZrO_2	KOH	4	42[b]
5	Nano-MgO-ZrO_2	KOH	4	68[c]
6	Nano-MgO-ZrO_2	KOH	4	92
7	Nano-MgO	KOH	4	46[13]
8	Nano-ZrO_2	KOH	4	25[13]
9	Normal MgO-ZrO_2	KOH	4	60[14b]

[a] Reaction conditions: acetophenone (1 mmol), KOH (2 mmol), IPA (3 mL), temp. 80 °C, catalyst (30 mg). [b] 10 mg catalyst used. [c] 20 mg catalyst used. [d] NR. No reaction.

The effect of reaction time was inspected for the reduction of acetophenone; notably nano-MgO–ZrO_2 gives almost quantitative yield of **2a** in 92% within 4 h; however within 5 h time, the yield of 1-phenylethanol has not increased further (93%). Therefore, the reaction time of 4 h was optimal for the reduction of acetophenone to 1-phenyl ethanol (Fig. 5).

In all cases the reaction was completed within 4–6 h with remarkably high yields (89–93%). As depicted in Table 2, selective reduction of 4-methoxyacetophenone (entry 4) is possible to afford the corresponding alcohol in excellent yield (93%) although with a slightly longer reaction time. Moreover, high yields can also be attained for 4-chloroacetophenone and 4-bromoacetophenone reduction (Table 2, entries 2 and 3), with no evidence of dehalogenation. The effectiveness of this protocol is comparable to some existing protocols[22] with the main advantages of being recyclable for several runs and the nanocatalysts being prepared from inexpensive precursors.

Table 2 Nano-MgO–ZrO_2 catalyzed ketone reduction[a]

Entry	Carbonyl compound (**1**)	Products (**2**)	Time (h)	Yield (%)
1	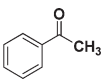	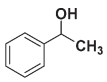	4	92
2	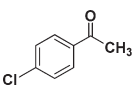	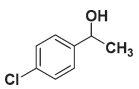	4.5	89
3	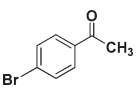	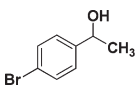	4.5	90
4	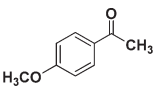	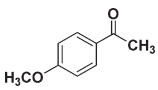	6	93
5			4	92

[a] Reaction conditions: carbonyl compound (1 mmol), KOH (1.5 mmol), 80 °C, IPA (3 mL), 30 mg of catalyst.

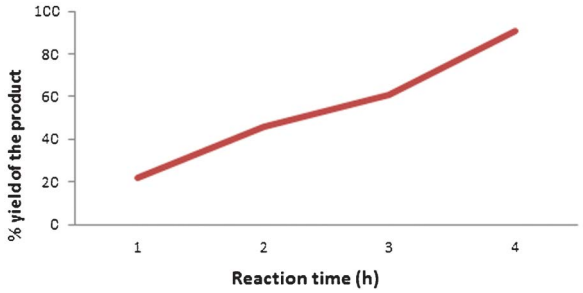

Fig. 5 Time dependency of carbonyl group reduction of acetophenone.

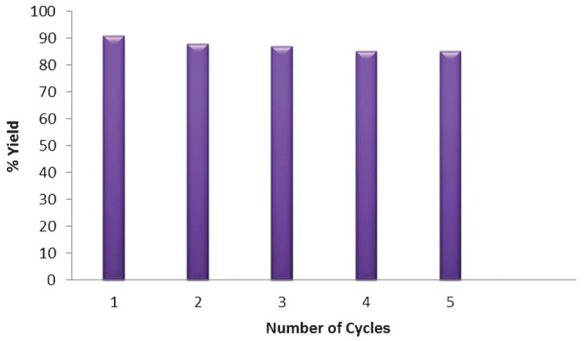

Fig. 6 Reusability study for the catalytic activity of nano-MgO–ZrO_2 catalyst.

A base supported Oppenauer oxidation mechanism should be involved (Scheme 3). This type of oxidation is known to be conducted among others using heterogeneous catalysts (*e.g.* alumina, zeolites).[23] Both carbonyl compound (ketone) and the alcohol (IPA) are bound to the catalyst (I). The alcohol is bound as the alkoxide. Coordination of the ketone to the catalyst activates it for the hydride transfer from the alkoxide followed by alcoholysis.

In order to prove that the reaction is heterogeneous, a standard leaching experiment was conducted by the filtration method. The model reaction of acetophenone (Table 2, entry 1) proceeded for 15 min in the presence of a nano-MgO–ZrO_2 at 80 °C. The reaction mixture was then filtered under suction to remove the catalyst. The filtered reaction mixture was then stirred without catalyst for 12 h. Notably, no formation of corresponding product was observed even after 12 h, indicating that no homogeneous catalyst was involved. The reusability of the catalyst was tested for the reduction of acetophenone. Under the established conditions the catalyst was filtered off after completion of the reaction and the reaction mixture was washed with water, followed by ethyl acetate, and then dried at 120 °C for 3 h, before being reused for the next cycle. The catalytic activity was maintained practically constant with only a slightly decrease even after the fifth cycle (Fig. 6).

To explore the catalytic activity of nano-MgO–ZrO_2, we tested it in the multicomponent reaction depicted in Scheme 4.

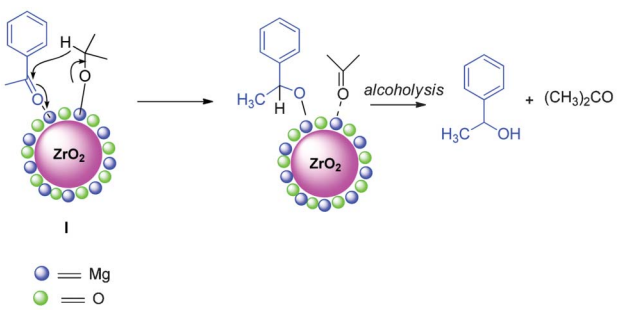

Scheme 3 Proposed mechanism for the reduction of acetophenone.

The reaction between benzaldehyde, ammonium acetate, methyl acetoacetate and 5,5-dimethylcyclohexane-1,3-dione, performed in the presence of nano-MgO–ZrO_2 under mild conditions, allowed us to obtain methyl 2,7,7-trimethyl-5-oxo-4-phenyl-1,4,5,6,7,8-hexahydroquinoline-3-carboxylate (**3**) in 95% yield.

In conclusion, we have investigated the surface properties of a MgO–ZrO_2 nano-catalyst by SIMS techniques, and observed that MgO is supported on ZrO_2. Furthermore, the catalytic activity of nano-MgO–ZrO_2 was investigated, for the reduction of carbonyl compounds by a simple procedure. In addition, the applicability of nano MgO–ZrO_2 was explored for four component reactions under benign conditions. This developed green protocol offers several advantages such as use of a heterogeneous and reusable catalyst, high reaction rates, operational simplicity and mild reaction conditions.

Experimental

All commercial reagents were used as received unless otherwise mentioned. For analytical and preparative thin-layer chromatography, Merck, 0.2 mm and 0.5 mm Kieselgel GF 254 percoated were used, respectively.

Synthesis of nano-MgO–ZrO_2

In a typical experiment, for the preparation of MgO–ZrO_2 an appropriate amount of magnesium nitrate [$Mg(NO_3)_2{\cdot}6H_2O$] (3.10 g) and zirconium oxychloride [$ZrOCl_2{\cdot}8H_2O$] (8.11 g) were dissolved together in a 2 L flask with 1 L deionized water. Dilute ammonia solution was added drop wise with vigorous stirring (RPM-5 000) until the precipitation was complete (around 6 to 8 h at pH = 10.0). The resultant precipitate was filtered and washed with distilled water until it was free from chloride ions. The residue was dried for 24 h at 383 K in an oven and the obtained precipitate of metal hydroxides was heated in a porcelain crucible progressively to 873 K for 10 h (ESI†).

Characterization nano-MgO–ZrO_2

After calcination, the nano-MgO–ZrO_2 catalyst was characterized by various analytical and spectroscopic techniques. The X-ray powder diffraction pattern was obtained using a

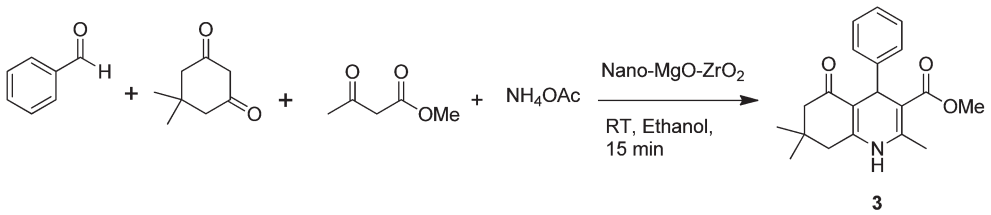

3

Scheme 4 Synthesis of methyl 2,7,7-trimethyl-5-oxo-4-phenyl-1,4,5,6,7,8-hexahydroquinoline-3-carboxylate (**3**).

conventional powder diffractometer (Philips 1050) using graphite monochromatized Cu-Kα radiation operating in Bragg–Brentano ($\theta/2\theta$) geometry. Transmission Electron Microscopy (TEM) experiments were performed on a Hitachi 8100 microscope with a Rontec standard EDS detector and digital image acquisition. All samples were prepared by evaporating dilute suspensions on a carbon-coated film. To produce a plain and conductive sample suitable for SIMS analysis, the powder catalyst was pressed onto an ultra-pure indium foil by Goodfellow (Huntingdon, UK). We used a manual toggle pressing machine by Brauer (Milton Keynes, UK). TOF-SIMS analysis was performed by acquiring positive and negative secondary ion spectra in the mass range of 0.5–200 *m*/*z* with an upgraded VG Ionex IX23LS TOF-SIMS set-up based on the Poschenrieder design. A focused liquid Ga^+ gun in the pulsed mode (6 kHz/40 ns) was used as a source of the analysis ions. The beam current in the continuous mode at 14 keV was *ca.* 15 nA with a raster size of 300 × 300 μm^2 (128 × 128 pixels, 10 kHz). The sample potential was ±5 kV. Vacuum during the experiments was maintained in the range of (2–3) × 10^{-9} mbar in the analytical chamber.

Reduction of carbonyl compounds (1)

Carbonyl compound **1** (10 mmol), IPA (10 mL), KOH (20 mmol) and nano-MgO–ZrO_2 (30 mg with respect to **1**), were stirred at 80 °C for an appropriate time. After completion of the reaction (monitored by TLC) the catalyst was separated by simple filtration. The resultant product was extracted with ethyl acetate from the reaction mixture. Then the organic solvent was evaporated *in vacuo*. The crude product was purified by column chromatography on silica gel using *n*-hexane and ethyl acetate as eluent. All compounds are well characterized and well reported in the literature.

Synthesis of methyl 2,7,7-trimethyl-5-oxo-4-phenyl-1,4,5,6,7,8-hexahydroquinoline-3-carboxylate (3)

A solution of benzaldehyde (5 mmol), 5,5-dimethylcyclohexane-1,3-dione (5 mmol), ammonium acetate (10 mmol), methyl acetoacetate (5 mmol), and nano-MgO–ZrO_2 (30 mg) in ethanol (3 mL) was stirred at room temperature for 20 min. After terminus of the reaction monitored by TLC (*n*-hexane and ethyl acetate; 70 : 30), the catalyst was filtered. To the solution was added ethyl acetate (10 mL). The organic layer was washed with saturated $NaHCO_3$ (aq) and brine, dried with anhydrous Na_2SO_4, and concentrated to dryness. The crude mixture was purified by crystallization in ethanol and the methyl 2,7,7-trimethyl-5-oxo-4-phenyl-1,4,5,6,7,8-hexahydroquinoline-3-carboxylate **3** was obtained in 95% yield.

Acknowledgements

This work has been supported by Fundação para a Ciência e Tecnologia through grants nos. PEst-C/EQB/LA0006/2011 and PEst-C/CTM/LA0025/2011. Manoj B. Gawande also thanks the PRAXIS program for the award of research fellowship SFRH/BPD/64934/2009.

References

1 (*a*) C. Mercier and P. Chabardes, *Stud. Surf. Sci. Catal.*, 1993, **78**, 677; (*b*) Y. Izumi, N. Natsume, H. Takamine, I. Tamaoki and K. Urabe, *Bull. Chem. Soc. Jpn.*, 1989, **62**, 2159–2164; (*c*) K. Tanabe and W. F. Holderich, *Appl. Catal., A*, 1999, **181**, 399–434; (*d*) B. M. Reddy and A. Khan, *Catal. Rev. Sci. Eng.*, 2005, **47**, 257–296.

2 (*a*) H. H. Kung, *Transition Metal Oxides: Surface Chemistry and Catalysis, Stud. Surf. Sci. Catal*, Elsevier, Amsterdam, 1989, Vol. 45, pp. 1–277; (*b*) V. E. Henrich and P. A. Cox, *The Surface Science of Metal Oxides*, Cambridge University Press, Cambridge, UK, 1994; (*c*) C. Noguera, *Physics and Chemistry at Oxide Surface*, Cambridge university press, Cambridge, UK, 1996; (*d*) S. U. Sonavane, M. B. Gawande, S. S. Deshpande and R. V. Jayaram, *Catal. Commun.*, 2007, **8**, 1803–1806.

3 M. B. Gawande, R. K. Pandey and R. V. Jayaram, *Catal. Sci. Technol.*, 2012, **2**, 1113–1125 and references cited therein.

4 M. J. Guittet, J. P. Crocombette and M. Gautier-Soyer, *Phys. Rev. B: Condens. Matter*, 2001, **63**, 125117–6.

5 F. S. Galasso, *Structure, Properties and Preparation of Perovskite-Type Compounds*, Pergamon Press, Oxford, 1969.

6 L. G. Tejuca, J. L. G. Fierro and J. M. D. Tascon, *Adv. Catal.*, 1989, **36**, 237–328.

7 Jin Huang and Qing Wan, *Sensors*, 2009, **9**, 9903–9924.

8 (*a*) S. U. Sonavane and R. V. Jayaram, *Synlett*, 2004, **1**, 146–148; (*b*) M. A. Pena and J. L. G. Fierro, *Chem. Rev.*, 2001, **101**, 1981–2017; (*c*) H. Kanai, Y. Ikeda and S. Imamura, *Appl. Catal., A*, 2003, **247**, 185–191; (*d*) S. K. Samantaray and K. Parida, *Appl. Catal., A*, 2001, **220**, 9; (*e*) S. D. Jackson and J. S. J. Hargreaves, *Metal Oxide Catalysis*, Wiley-VCH, 2008, ISBN-10: 3527318151; (*f*) G. Mestl, *Top. Catal.*, 2006, **38**, 69–82; (*g*) J. Kaspar, P. Fornasiero and M. Graziani, *Catal. Today*, 1999, **50**, 285–298; (*h*) R. Di Monte and J. Kaspar, *Top. Catal.*, 2004, **28**, 47–57; (*i*) R. Di Monte and J. Kaspar, *J. Mater. Chem.*, 2005, **15**, 633–648 and references cited therein.

9 (*a*) R. C. Larock, *Organic Transformations*, VCH, New York, 1989, p. 411; (*b*) G. W. Kabalka and R. S. Varma, *Comprehensive Organic Synthesis*, ed. B. M. Trost and I. Fleming, Pergamon Press, Oxford, 1991, vol. 8, pp. 363; (*c*) F.-Z. Su, L. He, J. Ni,

Y. Cao, H.-Y. He and K.-N. Fan, *Chem. Commun.*, 2008, 3531–3533.

10 (*a*) E. J. Creyghton, J. Huskens, J. C. Van der Waal and H. Van Bekkum, 1997, *Heterogeneous catalysis and fine chemicals IV*, Elsevier, Amsterdam, pp. 531–537; (*b*) Y. Ishii, T. Nakano, A. Inada, Y. Kishigami, K. Sakurai and M. Ogawa, *J. Org. Chem.*, 1986, **51**, 240–242.

11 D. J. Pasto, *J. Am. Chem. Soc.*, 1979, **101**, 6852–6857.

12 M. B. Gawande, P. S. Branco, K. Parghi, J. J. Shrikhande, R. K. Pandey, C. A. A. Ghumman, N. Bundaleski, O. M. N. D. Teodoro and R. V. Jayaram, *Catal. Sci. Technol.*, 2011, **1**, 1653–1664.

13 M. B. Gawande, S. N. Shelke, A. Rathi, P. S. Branco and R. K. Pandey, *Appl. Organomet. Chem.*, 2012, **26**, 395–400.

14 (*a*) M. B. Gawande and P. S. Branco, *Green Chem.*, 2011, **13**, 1355–3359; (*b*) M. B. Gawande and R. V. Jayaram, *Catal. Commun.*, 2006, **7**, 931–935; (*c*) S. N. Shelke, G. R. Mhaske, V. D. B. Bonifácio and M. B. Gawande, *Bioorg. Med. Chem. Lett.*, 2012, **22**, 5727–5730; (*d*) M. B. Gawande, V. Polshettiwar, R. S. Varma and R. V. Jayaram, *Tetrahedron Lett.*, 2007, **48**, 8170–8173.

15 (*a*) M. B. Gawande, S. S. Deshpande, S. U. Sonavane and R. V. Jayaram, *J. Mol. Catal. A: Chem.*, 2005, **241**, 151–155; (*b*) M. B. Gawande, S. S. Deshpande, J. R. Satam and R. V. Jayaram, *Catal. Commun.*, 2007, **8**, 576–582.

16 (*a*) M. B. Gawande, A. Velhinho, I. D. Nogueira, C. A. A. Ghumman, O. M. N. D. Teodoro and P. S. Branco, *RSC Adv.*, 2012, **2**, 6144–6149; (*b*) M. B. Gawande, A. Rathi, I. D. Nogueira, C. A. A. Ghumman, N. Bundaleski, O. M. N. D. Teodoro and P. S. Branco, *Chem Plus Chem*, 2012, **77**, 865–871; (*c*) M. B. Gawande, A. Rathi, P. S. Branco, I. D. Nogueira, A. Velhinho, J. J. Shrikhande, U. U. Indulkar, R. V. Jayaram, C. A. A. Ghumman, N. Bundaleski and O. M. N. D. Teodoro, *Chem.–Eur. J.*, 2012, **18**, 12628–12632; (*d*) M. B. Gawande, H. Guo, A. K. Rathi, P. S. Branco, Y. Chen, R. S. Varma and D. L. Peng, *RSC Adv.*, 2013, **3**, 1050–1053; (*e*) U. U. Indulkar, S. R. Kale, M. B. Gawande and R. V. Jayaram, *Tetrahedron Lett.*, 2012, **53**, 3857–3860; (*f*) M. B. Gawande, P. S. Branco, I. D. Nogueira, C. A. A. Ghumman, N. Bundaleski, A. Santos, O. M. N. D. Teodoro and R. Luque, *Green Chem.*, 2013, DOI: 10.1039/c3gc36844k.

17 (*a*) F. De Smet, M. Devillers, C. Poleunis and P. Bertrand, *J. Chem. Soc., Faraday Trans.*, 1998, **94**, 941–947; (*b*) J. Grams, J. Góralski and P. Kwintal, *Int. J. Mass Spectrom.*, 2010, **292**, 1–6; (*c*) N. Kruse and S. Chenakin, Low Energy Ion Scattering and Secondary Ion Mass Spectrometry, in *Characterization of Solid materials and Heterogeneous Catalysts*, ed. M. Che and J. C. Vedrine, 2012, Wiley, Weinheim, pp. 453–510.

18 (*a*) C. A. A. Ghumman, O. M. T. Carreira, A. M. C. Moutinho, A. Tolstogouzov, V. Vassilenko and O. M. N. D. Teodoro, *Rapid Commun. Mass Spectrom.*, 2010, **24**, 185–190; (*b*) C. A. A. Ghumman, A. M. C. Moutinho, A. Tolstogouzov and O. M.N. D. Teodoro, *Rapid Commun. Mass Spectrom.*, 2011, **25**, 997–999; (*c*) F. H. Field, *J. Phys. Chem.*, 1982, **86**, 5115–5123.

19 (*a*) D. R. Baer, M. H. Engelhard, A. S. Lea, P. Nachimuthu, T. C. Droubay, J. Kim, B. Lee, C. Mathews, R. L. Opila, L. V. Saraf, W. F. Stickle, R. M. Wallace and B. S. Wright, *J. Vac. Sci. Technol., A*, 2010, **28**, 1060–1072.

20 (*a*) G. K. Pradhan and K. M. Parida, *Intern. J. Engin. Sci. and Techn*, 2010, **2**, 53–65; (*b*) M. Zhang, T. An, X. Hu, C. Wang, G. Sheng and J. Fu, *Appl. Catal., A*, 2004, **260**, 215–222; (*c*) M. Zhang, G. Sheng, J. Fu, T. An, X. Wang and X. Hu, *Mater. Lett.*, 2005, **59**, 3641–3644.

21 K. Yamaguchi, K. Ebitani, T. Yoshida, H. Yoshida and K. Kaunda, *J. Am. Chem. Soc.*, 1999, **121**, 4526–4527.

22 (*a*) F.-Z. Su, L. He, J. Ni, Y. Cao, H.-Y. He and K.-N. Fan, *Chem. Commun.*, 2008, 3531–3533; (*b*) F. Alonso, P. Riente, F. Rodriguez-Reinoso, J. Ruiz-Martinez, A. Sepffllveda-Escribano and M. Yus, *ChemCatChem*, 2009, **1**, 75–77.

23 E. J. Creyghton, S. D. Ganeshie, R. S. Downing and H. van Bekkum, *J. Mol. Catal. A: Chem.*, 1997, **115**, 457–472.